ACS OMEGA

Open Access

http://pubs.acs.org/journal/acsodf

Article

Synergistic Elimination of Chlorophenols Using a Single-Atom Nickel with Single-Walled Carbon Nanotubes: The Roles of Adsorption, Hydrodechlorination, and the Electro-Fenton Process

Xinlong Pei,[⊥] Baitao Chen,[⊥] Zehui Wang, Chenhong Ma, Long Li, Yonghong Li, Xiaoxiong Huang,* Xiaolong Yao, and Hong Zhu*

Cite This: *ACS Omega* 2024, 9, 37910−37922

Read Online

ACCESS | Metrics & More | Article Recommendations | Supporting Information

ABSTRACT: Electrocatalytic degradation enables the efficient treatment of chlorinated pollutants (COPs); however, its application has been significantly hindered by the large amounts of unsafe intermediate products. In this study, we present a single-atom nickel with single-walled carbon nanotubes (SWCNTs) as an electrochemical reactor for the complete elimination of chlorophenols. Distinct products and reductive mechanisms were observed for Ni−N−C compared to Cu−N−C. Ni−N−C incorporation has a novel degradation pathway for efficient chlorophenol degradation involving hydrodechlorination and the electro-Fenton process. Most importantly, the weak adsorption between the chlorophenols and the SWCNTs promoted their dechlorination by the attached active atomic hydrogen (H*) formed on the Ni−N−C. Meanwhile, the SWCNTs improved the reduction of O_2 to H_2O_2, which was subsequently decomposed by Ni−N−C to form hydroxyl radicals (·OH) for phenol oxidation. As a result, the degradation rate of 4-chlorophenol was increased by 5 and 10 times compared with those of the Ni−N−C and SWCNTs alone, respectively. The first-order reaction rate constant was 2.7 h^{-1}, and the metal mass kinetics constant was 1956.5 $min^{-1}g^{-1}$. Aromatic COPs containing benzene rings could be degraded, but chloroacetic acids could not. This study demonstrates a new design for multifunctional electrochemical degradation that functions via dechlorination and the ·OH activation mechanism.

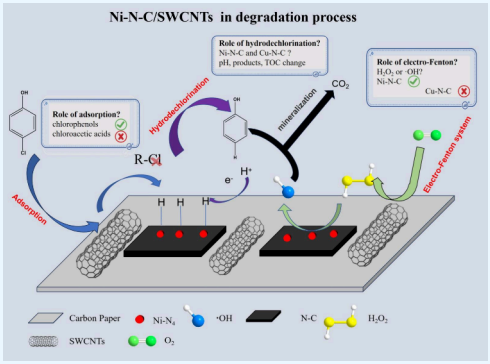

1. INTRODUCTION

Chlorinated organic pollutants (COPs) are often used as insecticides, industrial raw materials, and chemical synthetic products.[1] They are toxic and difficult to biodegrade because of the presence of chlorine atoms. Therefore, many COPs are listed as priority pollutants in the Stockholm Convention.[2−4] Owing to their persistent organic pollutant characteristics, electrochemical processes exhibit high efficiency in the detoxification and degradation of these pollutants.[5,6] Hydrogen reduction dechlorination (HRD)[7] and the electro-Fenton process (EF)[8] are the main approaches used to degrade COPs. The EF occurs in situ to produce H_2O_2. Although it can disrupt the molecular structure, the presence of chlorine atoms leads to low-current utilization. HRD forms adsorbed atomic hydrogen (H*), which is substituted by the chlorine atoms of COPs.[9,10] The incomplete degradation may result in an unsatisfactory decrease in the toxicity. A combination of HRD with EF was also used to attempt to remove COPs, including cathode materials such as Fe/Cu bimetallic single-atoms and atomic Fe and Co.[11−13] Herein, Fe is identified as the main material for EF; however, the specific roles of the materials in HRD and EF remain unclear, as indicated by the limited research on the topic.[14−16] There is a need to develop new cathodic materials that effectively integrate HRD and EF for the degradation of COPs.[9,16,17]

Single-atom metals have been extensively studied in the field of heterogeneous catalysis due to their high dispersibility and catalytic activity.[2,18,19] Notable examples include Fe SACs[20] and Co SACs.[21] All of these metals have demonstrated extraordinary electrocatalytic performance in EF.[11,22] Additionally, atomic Fe−N−C, Co−N−C, and Pd−N−C have also been reported for their efficiency in dechlorination.[19,23,24] However, existing research has solely focused on cathodic materials, with limited attention given to the structure of COPs. The relationship between the catalytic roles of the cathodic materials and the target degradation products of COPs still remains unclear.

Atomic nickel has been reported to activate hydrogen (H*) for COP dechlorination.[5] Our previous research also revealed

Received: May 5, 2024
Revised: August 1, 2024
Accepted: August 5, 2024
Published: August 26, 2024

that metal Ni activated H* for COP dechlorination, which is notably different from that observed in Cu.[25] Herein, we chose atomic Ni and atomic Cu electrodes to further explore the differences between the two and dechlorination pathways. In addition, due to the pi−pi conjugation between chlorophenols and SWCNTs, chlorophenols may react with H* on the atomic metal to achieve dechlorination. In this study, the atomic metal was physically complexed with SWCNTs as the reduction−oxidation complex on the cathode catalyst. Throughout the process, COPs undergo complete dechlorination and mineralization by the reduction of HRD and oxidation-mediated EF. This study represents the first attempt to determine the structure of COPs upon degradation and provides insights into three key steps in the synergistic degradation of chlorophenols, including adsorption, dechlorination, and EF with ·OH radicals. The in situ generation of H_2O_2 by O_2 reduction is crucial, followed by the effective activation of H_2O_2 to ·OH radicals.[13,26,27] Thus, far, the active sites for the two steps in forming ·OH radicals remain unclear.[28] While some single-atom metals have been reported to have both effects, this study found that the formation of H_2O_2 and its decomposition to ·OH radicals occur at two different reaction points. Nitrogen-doped graphene promoted the formation of H_2O_2, and single-atom Ni decomposed to ·OH radicals.

We aim to enhance COP degradation by using SWCNTs to disperse Ni−N−C. Pi−pi absorption occurred between the benzene rings on the COPs and the SWCNTs, and then, the nearby Ni−N−C completed the degradation of COPs by HRD and the EF. Ni−N−C and SWCNTs were used to create a cathode with three collaborative functions (adsorption, HRD, and the EF). A detailed mechanistic study of the synergistic effects of the SWCNTs and Ni−N−C on the degradation of chlorophenols and phenols in three different roles was conducted, and the differences between Ni−N−C and Cu−N−C were compared, as were the differences between aliphatic and aromatic COPs. Electrochemical experiments, electron paramagnetic resonance spectroscopy (EPR), and density functional theory (DFT) calculations were conducted to demonstrate the key active sites of three roles (adsorption, HRD, and the EF). Through experimental data and theoretical analysis, a possible new mechanism of COPs degradation was postulated.

2. MATERIALS AND METHODS

2.1. Materials. Nickel nitrate hexahydrate and copper nitrate monohydrate, both of analytical grade, were purchased from Beijing Chemical Industry Group Co. Ltd. (China). Ultrahigh-purity carboxylated SWCNTs (purity >95%, diameters: 1−2 nm) were purchased from Sigma-Aldrich (USA). 4-Chlorophenol (4-CP), 2-chlorophenol (2-CP), 2,4-dichlorophenol (2,4-DCP), chloroacetic acid (HAAs), and 1,2-dichloroacetic acid (DCA) were purchased from Yien Chemical Technology Co. Ltd. (Shanghai, China). A 5% DuPont Nafion membrane solution and Nafion 117 ion membranes were purchased from Sanshe Industrial Co. Ltd. (Shanghai, China). Potassium ferricyanide ($K_3Fe(CN)_6$), potassium chloride (KCl), 98% sulfuric acid (H_2SO_4), and sodium hydroxide (NaOH) were all purchased from Beijing Chemical Industry Group Co. Ltd. Phenol and anhydrous sodium sulfate (Na_2SO_4) were obtained from Xilong Chemical Co. Ltd. Methanol (MeOH), *tert*-butanol (TBA), *p*-benzoquinone, and potassium thiocyanate were obtained from Macklin. All of the reagents were of analytical grade and were used without additional purification. Deionized water was used in the preparation of all of the solutions, and all of the experiments were conducted at room temperature unless stated otherwise.

2.2. Synthesis of Ni−N−C, Cu−N−C, and N−C. Single-atom nickel and copper were prepared through a typical single-atom metal preparation method.[29] Detailed descriptions of the experiments are shown in the Supporting Information. Finally, Ni−N−C and Cu−N−C with different pyrolysis temperature catalysts were obtained as black powders. Terephthalic acid (10 mg) and dicyandiamide (100 mg) were milled, mixed, and annealed at 800 °C, and the resultant sample was named N−C at 800 °C.

2.3. Fabrication of Electrodes. First, 3 mg of materials (Ni−N−C, Cu−N−C, and N−C) was combined with different mass ratios of SWCNTs, dissolved in 30 μL of a Nafion solution (5%, DuPont) and 1 mL of an ethanol solution (50 wt %), and sonicated for 30−50 min to a homogeneous ink-like solution. Carbon paper (CP) (1 cm × 2 cm) was rinsed with an ethanol solution (50 wt %) and dried under an infrared lamp. Then, 1 mL of modification solution was dropped on CP and dried with an infrared lamp to obtain the CP/SWCNTs, CP/N−C, CP/SWCNTs/Ni−N−C, and CP/SWCNTs/Cu−N−C samples. For the electrochemical impedance spectroscopy (EIS) characterization, 3 μL of modification solution was dropped on 3 mm polished glassy carbon electrodes (GCEs) to obtain a series of electrodes, which were named GCE/SWCNTs, GCE/N−C, GCE/SWCNTs/Ni−N−C, and GCE/SWCNTs/Cu−N−C. Ni−N−C prepared at 800 °C and Cu−N−C prepared at 800 °C that represent the Ni- and Cu-modified electrode samples, respectively.

2.4. Material Characterization. The EIS method was used to analyze the electrochemical impedance spectra in concentrated solutions of potassium ferricyanide using a CHI660E electrochemical workstation (Chenhua Instrument, China). Scanning electron microscopy (SEM, Gemini SEM300) was used to evaluate the microscopic morphologies of the electrode surfaces. The elemental composition of the surfaces of the electrode materials was analyzed through X-ray photoelectron spectroscopy (XPS) using a Thermo Fisher Scientific Escalab 250Xi photoelectron spectrometer for N-elemental analysis, confirming the presence of single-atom metals and the form of their existence. Transmission electron microscopy (TEM) was performed using a TEM-F200. High-angle annular dark-field scanning transmission electron microscopy (HAADF-STEM) characterization was performed on a JEOL JEM-ARM 300F TEM system operating at 300 kV (Japan). The metal contents in the materials were determined by inductively coupled plasma-atomic emission spectrometry (ICP-AES). Ni K-edge X-ray absorption fine structure spectroscopy (XAFS) analysis was performed with Si(111) crystal monochromators at the BL14W Beamline at the Shanghai Synchrotron Radiation Facility (SSRF) (Shanghai, China). The spectra were processed and analyzed using Athena software.

2.5. Degradation Experiment. Electrochemical degradation experiments were conducted in a 50 mL single-compartment electrolyzer with 30 mL of 0.05 mol/L Na_2SO_4 solution at pH values in the range of 1−5. A three-electrode system was used to conduct the experiments, with the working electrode being the prepared modified electrode, the reference

https://doi.org/10.1021/acsomega.4c04289
ACS Omega 2024, 9, 37910−37922

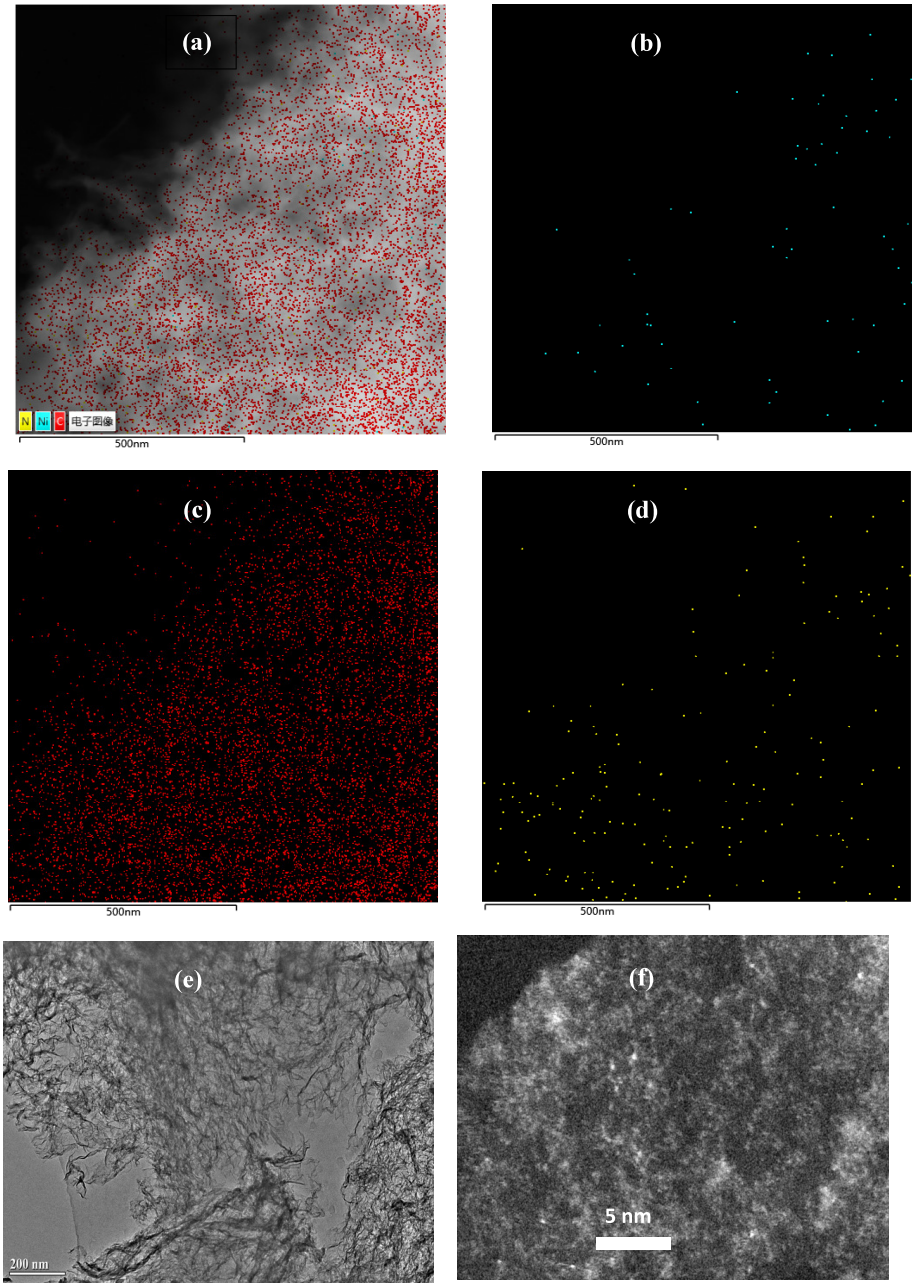

Figure 1. SEM-EDS results for Ni−N−C: (a) Ni + C + N, (b) Ni, (c) C, and (d) N. (e) TEM results for Ni−N−C and (f) high-angle annular dark-field scanning transmission electron microscopy (HAADF-STEM) results for Ni−N−C.

electrode (saturated calomel electrode (SCE)), and the anode being a 1 cm × 1 cm platinum sheet electrode, as shown in Figure S1. The power supply was provided by a Shanghai Chenhua Chi660e electrochemical workstation, and the amperometric *i*−*t* curves were obtained over a potential range of −1.4 to −0.8 V. The concentrations of the pollutants to be degraded (4-CP, 2-CP, 2,4-DCP, phenol, and chloroacetic acids) were 30 ppm. The device was placed on a magnetic stirrer; stirring was performed during the experiments, and air was pumped in during the reaction process (N_2 protection was used for comparison experiments). For sampling, samples (1 mL) were taken at set time points and filtered through a 0.22 μm organic filtration membrane for high-performance liquid chromatography (HPLC) analysis. For the modified composites, the ratio of nanocarbon materials, the synthesis temperatures for the single-atom metals, the electrolyte solution pH, and other related parameters were optimized.

3. RESULTS AND DISCUSSION

3.1. Structural and Electronic Properties of Ni−N−C and Cu−N−C. The catalysts were prepared by pyrolysis and structurally characterized using XPS and transmission electron microscopy−energy-dispersive X-ray spectroscopy (TEM-EDS) and transmission electron microscopy (TEM). The TEM-EDS for Ni−N−C (Figure 1a−d) showed that the C, N, and metal were uniformly distributed. The Cu−N−C also exhibited a uniform distribution (Figure S3a−e). The Ni and Cu contents were determined to be 1.3 and 2.6%, respectively, as shown in the EDS (Figure 1a and Figure S3b); these results

https://doi.org/10.1021/acsomega.4c04289
ACS Omega 2024, 9, 37910−37922

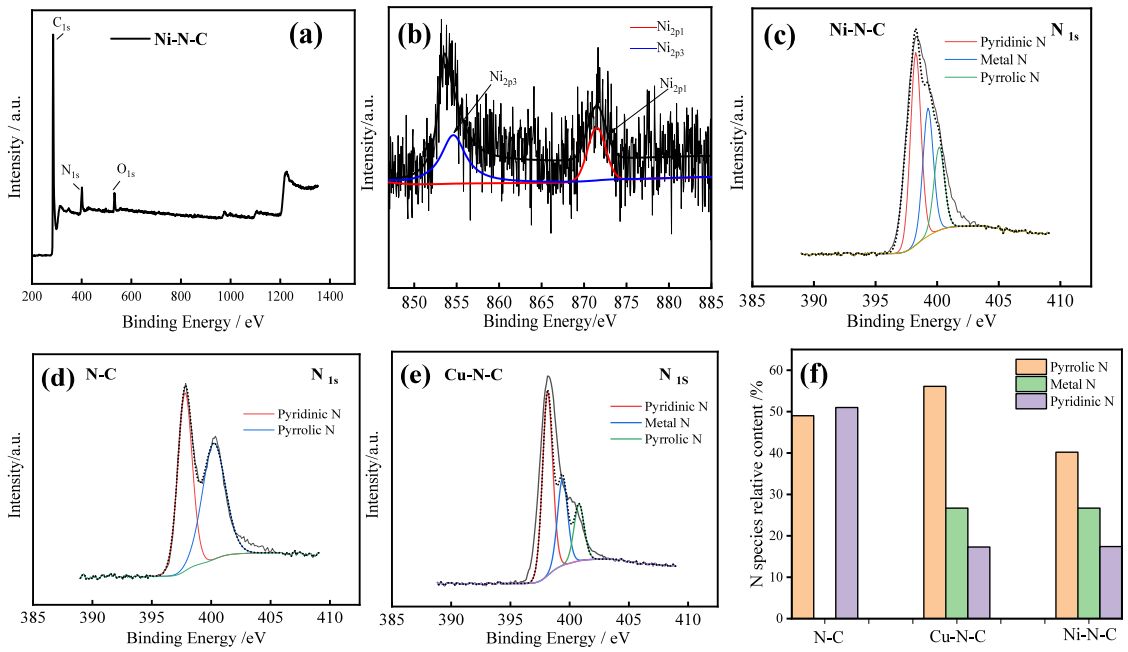

Figure 2. X-ray photoelectron spectroscopy (XPS) spectra: (a) survey spectra, (b) Ni 2p spectra for Ni−N−C, and (c−e) N 1s spectra. (f) Relative contents of N species in different catalysts.

are similar to the Ni contents observed in XPS (Figure 2a,b). TEM images showed that the metal−N−C exhibited a schistose shape resembling graphene (Figure 1e and Figure S3e). In the XPS spectra (Figure 2c−f), the N spectra of the Ni−N−C and Cu−N−C were fitted with peaks at 397.9, 398.9, and 400.2 eV, which were assigned to pyridinic N, metallic N, and pyrrolic N, respectively. These results indicate the successful incorporation of Ni and Cu into nitrogen-doped graphene (N−C), and they showed that the peaks of pyridinic N were decreased while those of metallic N were increased. XPS was used to analyze the Ni−N−C surface. The XPS spectra in Figure 2a−d clearly observe Ni, N, and C, indicating the presence of Ni on the catalyst surface. Through the Ni 2p orbital XPS spectra of Figure 2b, the Ni 2p3/2 and Ni 2p1/2 peaks were observed at 853 and 870 eV, respectively. After the metallic Ni or Cu was anchored, the pyridinic N was decreased (Figure 2f), the pyridinic N atoms in the catalysts acted as anchors to stabilize single-metal atoms, and Ni−N-*x* and Cu−N-*x* sites could form. All the obtained metal−N−C catalysts showed multilayer-sheet graphene-like structures (Figure S2c−f).

The coordination environment and chemical state of Ni in the metal−N−C were studied using atomic resolution HAADF-STEM and X-ray absorption near-edge spectroscopy (XANES) spectroscopy. HAADF-STEM revealed isolated bright dots, corresponding to the presence of metallic Ni (Figure 1f). Figure 3a shows the normalized XANES spectra of Ni−N−C from 800 °C and reference materials, including NiO and Ni foil.

The coordination environment of the Ni species in Ni−N−C was analyzed. The nickel absorption edge of Ni−N−C-800 °C (8320−8400 eV) is located between the nickel foil and nickel oxide at half the maximum intensity of the edge, and as reported, it suggested that the positively charged single Ni atoms were between Ni(0) and Ni(2+).[30] In the curve of Ni−N−C-800 °C, the weak pre-edge peaks between position at about 8333 eV and position at about 8339 eV were ascribed to the quadrupole-allowed transition of 1s to 3d and 1s → $4p_z$ transition.[31] This indicates the occurrence of the hybridization of 3d and 4p orbitals of Ni central atoms.[32] The strong peak (peak B) was characteristic of the square-planar configuration with D_{4h} centrosymmetry of Ni−N−C phthalocyanine-like moieties. That is, the Ni atoms coordinated with pyridinic N in the Ni−N−C.

More detailed information about nickel in Ni−N−C was obtained using Fourier-transform (FT) extended X-ray absorption fine structure spectroscopy (EXAFS). The Ni K-edge FT-EXAFS spectrum of Ni−N−C-800 °C exhibited a nearest-neighbor signal at 1.41 Å corresponding to Ni−N−C, similar to the signal of tetrahedral coordination (Ni−N_4).[30] As shown in Figure 3b, the Ni−Ni coordination peak at 2.15 Å does not appear in the Ni K-edge FT-EXAFS spectra of Ni−N−C, which showed that no Ni nanoclusters are formed. EXAFS wavelet transform analysis can distinguish back-scattered atoms that could overlap in R space and provide the radical distance and K spatial resolution.[32] A quantitative least-squares fitting of the EXAFS data was performed to analyze the coordination configuration of the Ni atoms in the Ni−N−C, and the coordination parameters is shown in Table S1. The coordination number of the Ni−N bond in Ni−N−C was determined to be about 4.

Totally, the X-ray absorption characteristics of the Ni−N−C at 800 °C catalyst confirmed the successful preparation of single-atom nickel doping on nitrogen-doped carbon.[31] Metal−N−C was complexed with the SWCNTs. The SEM images of the two mixed materials showed that the tubular SWCNTs and the metal−N−C sheet were uniformly mixed and orderly arranged (Figure S2e,f). The composite materials were physically modified on conductive CP to conduct the COP degradation experiments.

3.2. Chlorinated Organic Pollutant Degradation with Metal−N−C Cathodes. The composition of the catalytic cathode was found to affect the degradation of 4-CP. The 4-CP degradation experiments were carried out in a continuously

https://doi.org/10.1021/acsomega.4c04289
ACS Omega 2024, 9, 37910−37922

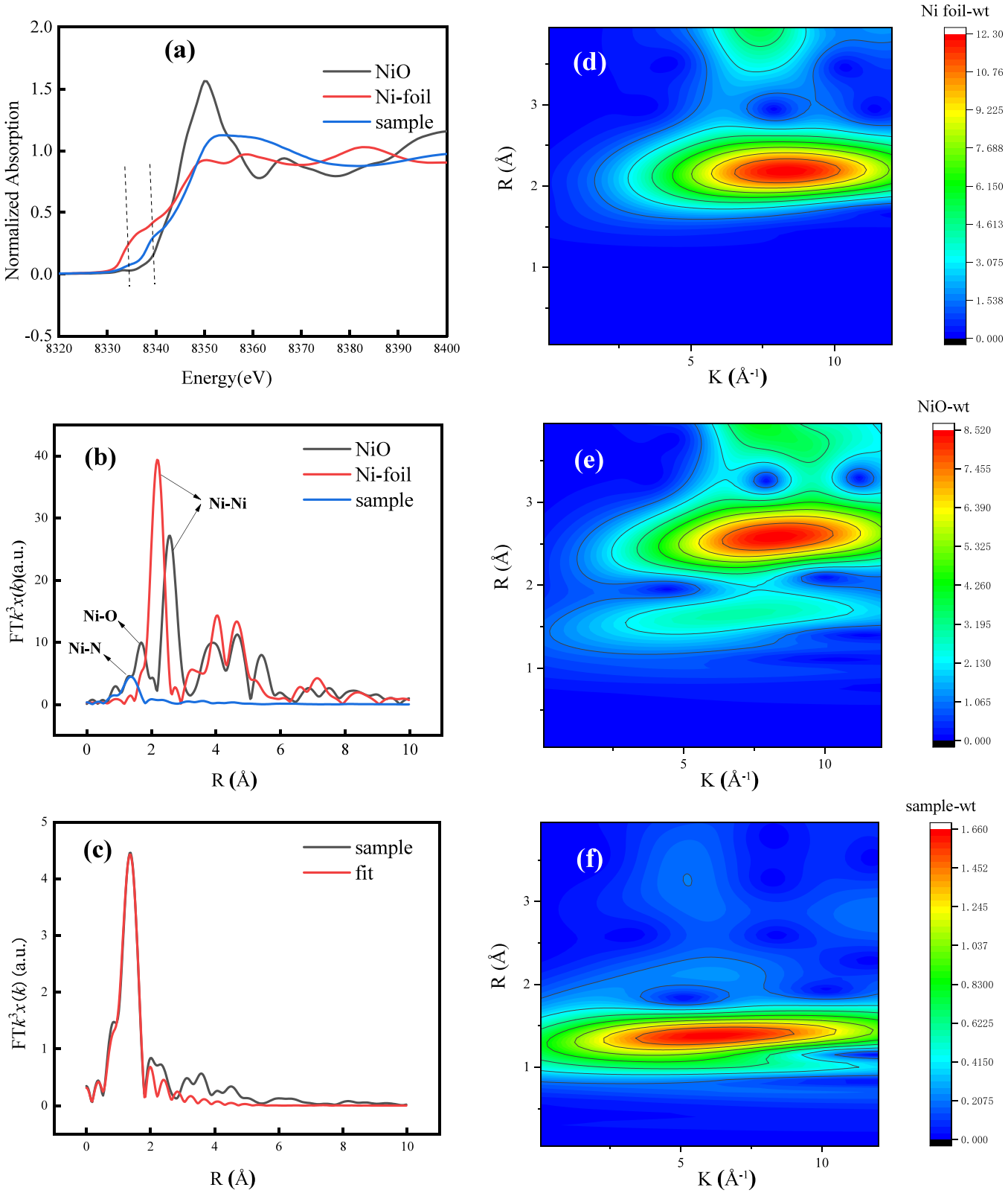

Figure 3. (a) X-ray absorption near edge spectroscopy (XANES) spectra and (b) Fourier-transform extended X-ray absorption fine structure spectroscopy (FT-EXAFS) spectra. NiO of the Ni−N−C and Ni foil tested at (c) the Ni K-edge and (d−f) the wavelet transform (WT).

aerated single chamber reactor. Figure 4a shows the 4-CP degradation curves with the reaction time for the CP, CP/N−C, CP/SWCNTs, CP/SWCNTs/Ni−N−C, and CP/SWCNTs/Cu−N−C samples. As shown in Figure 5, the influence of pH for the degradation was complex; here, we chose pH of 7 to evaluate materials. Among these catalysts, CP/SWCNTs/Ni−N−C exhibited the best activity, with 95% removal efficiency in 60 min. The first-order reaction kinetics parameter (K_{obs}) of the CP/SWCNTs/Ni−N−C sample was 2.7 h^{-1}, which was considerably higher than that of the CP

https://doi.org/10.1021/acsomega.4c04289
ACS Omega 2024, 9, 37910−37922

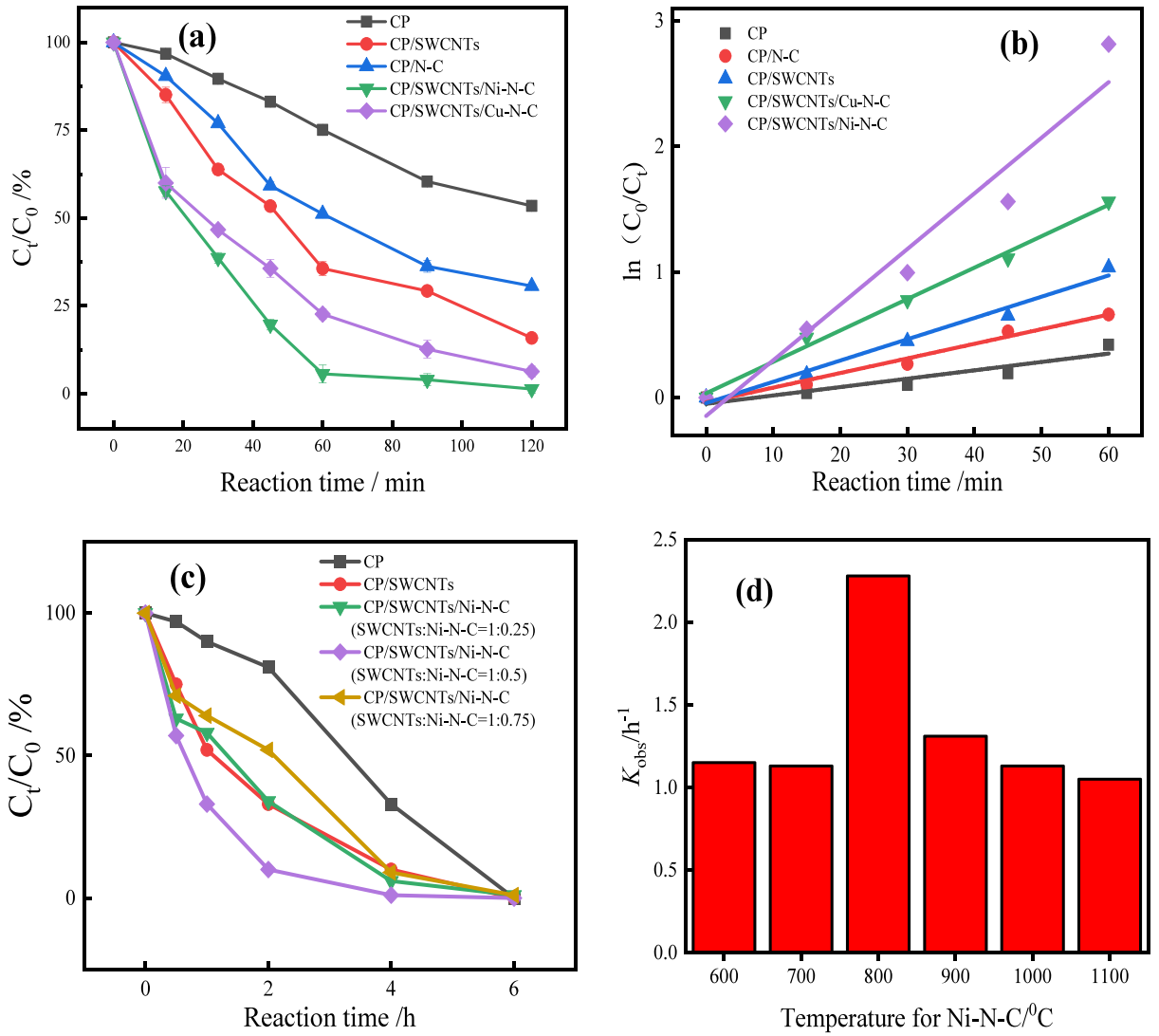

Figure 4. Electrode degradation of 4-CP: (a) degradation−time curves, (b) K_{obs} values of the first-order reaction rate constants, (c) degradation curves of different proportions of materials (*wt*%), and (d) comparison of the K_{obs} values of the degradation reaction of GP/SWCNTs/Ni−N−C (at different temperatures), pH = 7, 0.05 M sodium sulfate, and −0.8 V.

(0.40 h^{-1}), CP/N−C (0.70 h^{-1}), CP/SWCNTs (1.02 h^{-1}), and CP/SWCNTs/Cu−N−C (1.5 h^{-1}) samples, as shown in Figure 4b. In order to exclude the effect of adsorption and anodization, adsorption (no potential applied) and anodization experiments were conducted (adding a Nafion 117 ion exchange membrane to the anode and cathode electrolytic cells). After 120 min of treatment, no 4-CP was removed by the adsorption and anodic oxidation processes.

The results indicated that 4-CP was mainly degraded by the cathodic reaction process. The K_{obs} sequence indicated that 4-CP could be efficiently degraded by CP/SWCNTs/Ni−N−C. The effect of the SWCNTs and Ni−N−C with a mass ratio of 2:1 was the strongest (Figure 4c), indicating a synergistic effect between the two materials in the degradation of 4-CP. SEM also showed the dispersion of the SWCNTs and Ni−N−C (Figure S2e). The comparison of the dechlorination degradation of the Ni−N−C samples produced at different temperatures, from 600 to 1100 °C, showed that Ni−N−C prepared at 800 °C exhibited the optimal K_{obs} value (Figure 4d). The temperature affected the Ni−N coordination morphology, indicating that the morphology of the Ni−N−C sample prepared at 800 °C was the most favorable for the catalytic degradation of 4-CP. Therefore, the Ni−N−C sample prepared at 800 °C was subjected to material characterization and subsequent degradation experiments. Henceforth, "Ni−N−C" refers to the Ni−N−C sample prepared at 800 °C.

To further investigate the degradation mechanism of the CP/SWCNTs/Ni−N−C, electrochemical characterization was performed on these electrodes. The detection of potassium ferrocyanide is shown in Figure S4. The effective surface areas of the four modified electrodes were calculated using Formula 1.

$$I_p = 2.69 \times 10^5 An\sqrt{DnvC} \quad (1)$$

where n represents the number of electrons present in the redox half-reaction, v is the voltage scanning rate ($V{\cdot}s^{-1}$), A is the effective area of the electrode (cm^2), D is the diffusion coefficient, which is usually 6.057×10^{-6} $cm^2{\cdot}s^{-1}$ (25 °C), C is the concentration of $[Fe(CN_6)]^{3-/4-}$ ($mmoL{\cdot}L^{-1}$), and I_p is the peak redox current value. n for $[Fe(CN_6)]^{3-/4-}$ is 1. Simplifying the formula yields, $I_p = 3.310 \times 10^{-2} Av^{1/2}$. A linear regression equation was obtained by plotting and fitting the

https://doi.org/10.1021/acsomega.4c04289
ACS Omega 2024, 9, 37910−37922

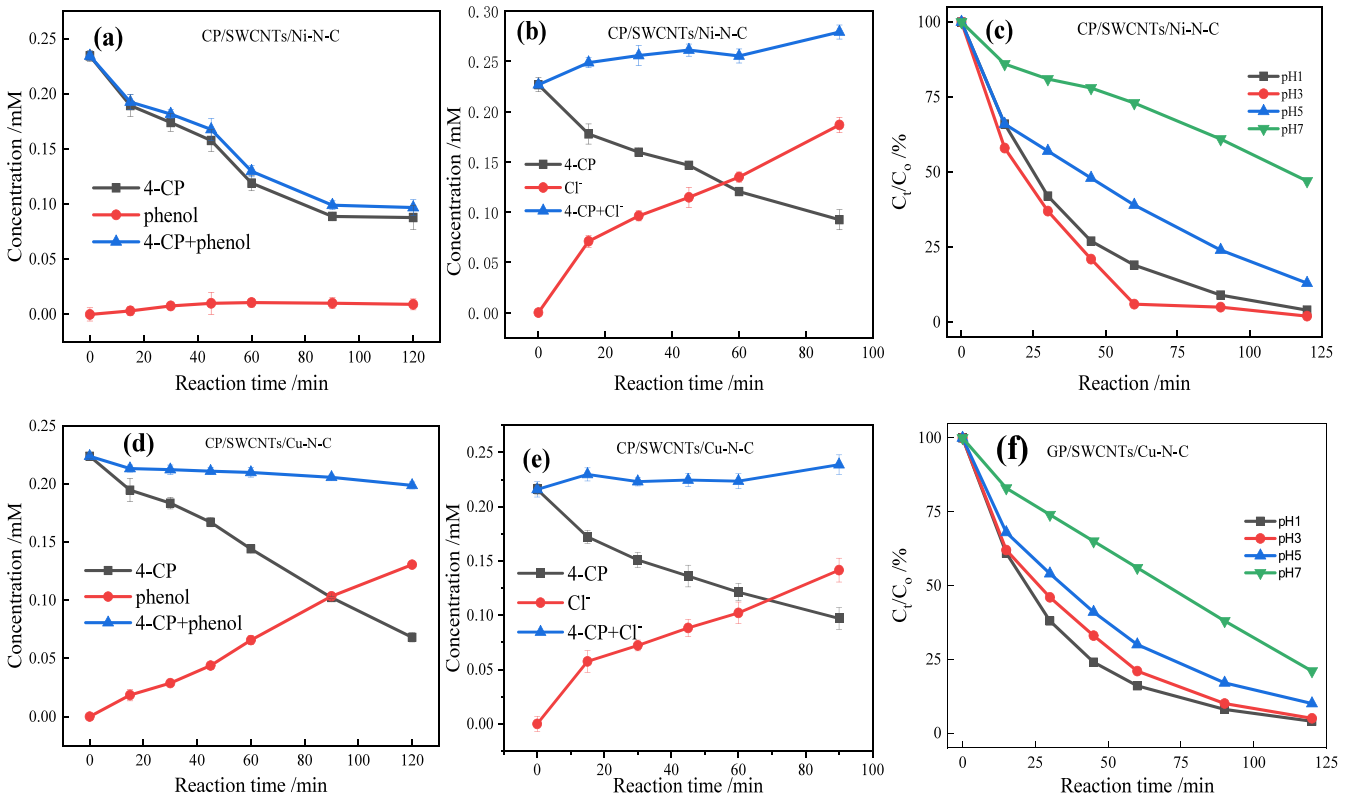

Figure 5. Electrode degradation of 4-CP plots: (a, b) product concentration changes during CP/SWCNTs/Ni−N−C degradation of 4-CP, (c) CP/SWCNTs/Ni−N−C degradation at different pH values, (d, e) product concentration changes during CP/SWCNTs/Cu−N−C degradation of 4-CP at pH = 5 and −1.4 V in 0.05 M sodium sulfate solution, and (f) CP/SWCNTs/Cu−N−C degradation at different pH values.

peak currents at logarithms of different sweep speeds (Figure S4a). Based on the slope of the regression equation, the effective surface areas of the four electrodes were 3, 81, 112, and 139 cm^2. The effective surface area of the electrode increased sequentially due to the modification of the SWCNTs and metal−N−C.

The potential window of the electrode plays an important role in its electrochemical properties, and the hydrogen and oxygen evolution of the electrode material will have an effect on the analyte. Therefore, polarization curve experiments (linear sweep voltammetry, LSV) were conducted on four modified electrodes to compare their hydrogen and oxygen evolution abilities. As shown in Figure S4b, the hydrogen and oxygen evolution abilities of the four electrodes were in the order of CP/SWCNTs/Ni−N−C > CP/SWCNTs/Cu−N−C > CP/SWCNTs > CP. The lower hydrogen evolution potential could allow CP/SWCNTs/Ni−N−C to produce hydrogen more easily. Using a GCE as the substrate instead of CP, the impedance values of the obtained electrodes were in the order of GCE > GCE/Cu−N−C > GCE/Ni−N−C > GCE/SWCNTs/Cu−N−C > GCE/SWCNTs/Ni−N−C > GCE/SWCNTs. There have been many reports mentioning the superiority of the SWCNTs and metal−N−C in improving catalytic performances and reducing the impedance, and these results are consistent with those of this experiment. However, it is interesting that the addition of metal−N−C (GCE/SWCNTs/Ni−N−C) yielded a greater impedance than that of the electrode with only SWCNT modification (GCE/SWCNTs) (Figure S4c), but the CP/SWCNTs/Ni−N−C showed superior performances in degrading 4-CP than the CP/SWCNTs. Therefore, it was inferred that the effect of the SWCNTs and metal−N−C on the 4-CP was not only a single electrocatalytic effect but also a more complex synergistic mechanism. We speculate that the adsorption of chlorophenol and the adsorption of active hydrogen played important roles in the degradation of the composite prepared by HRD and the EF. Interestingly, the degradation products of 4-CP by the CP/SWCNTs/Ni−N−C and CP/SWCNTs/Cu−N−C were also different. The comparative experiment of the Ni−N−C and Cu−N−C showed that different mechanisms were involved.

Although pH 3 is the optimal pH for CP/SWCNTs/Ni−N−C, we chose the pH of 5 to evaluate the maximum product concentration changes between the two materials. As shown in Figure 5a−f, at a nearly neutral pH (pH = 5), the degradation results of the Ni−N−C and Cu−N−C modified with CP were different. The product of 4-CP degradation by the CP/SWCNTs/Cu−N−C was almost only phenol, with the total carbon (phenol and remaining 4-CP) maintained at a constant concentration, and chloride ions also increased with the decrease in the 4-CP concentration, resulting in a constant total content (Cl^- concentration and remaining 4-CP). This indicates that under near-neutral conditions, the Cu−N−C-modified electrode exhibited a typical mechanism for hydrogen dechlorination, which is consistent with the general dechlorination literature reports. Initially, H* was formed, followed by dechlorination of the COPs, and the nine characteristic peaks of DMPO-H were observed in the reaction systems, as shown in Figure 6f. The degradation of COPs by the Cu−N−C-modified electrode continuously increased from pH = 7 to 1 (Figure 5f), as H* formation depends on the concentration of hydrogen ions. Due to its weak activation ability for active hydrogen, the Cu−N−C-modified electrode showed more

https://doi.org/10.1021/acsomega.4c04289
ACS Omega 2024, 9, 37910−37922

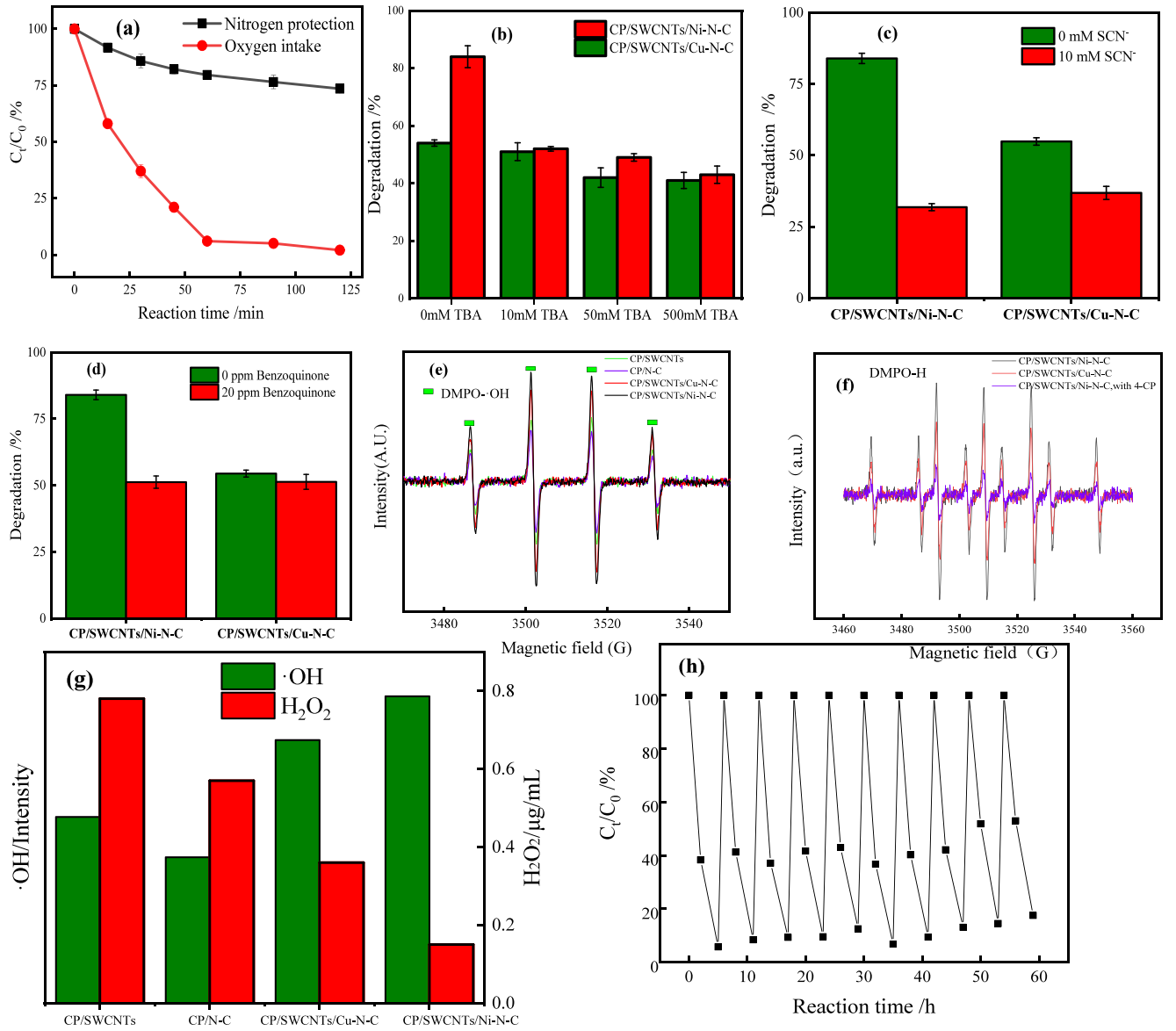

Figure 6. (a) Degradation curves of 4-CP by the CP/SWCNTs/Ni−N−C under different conditions, (b−d) effects of different media on electrode degradation of 4-CP (pH = 5, 0.05 M sodium sulfate, − 0.8 V), (e) EPR spectra of 5,5-dimethyl-1-pyrroline-*x*-oxide (DMPO)-OH, (f) DMPO-H detection by EPR spectra in various systems, (g) comparison of ·OH and H_2O_2 concentrations, and (h) degradation curves of CP/SWCNTs/Ni−N−C batch treatment with 10 batches of 4-CP degradation (pH = 3, 0.05 M sodium sulfate, − 0.8 V).

dependency on the pH.[33] A decrease in the pH caused an increase in degradation (Figure 5f). However, the Ni−N−C-modified electrode was different. Although the amount of Cl^- and remaining 4-CP was constant during the reaction, the total carbon (phenol and remaining 4-CP) was unbalanced (Figure 5a), indicating that phenol continued to degrade. The Ni−N−C electrode primarily exhibited hydrogen dechlorination. As shown in Figure 6f, the Ni−N−C electrode yielded more DMPO-H than the Cu−N−C electrode, and with the addition of 4-CP, the DMPO-H even disappeared. Furthermore, the Ni−N−C electrode exhibited a different mechanism from that of the Cu−N−C at pH 5, and oxidation reactions continued to occur after dechlorination.

More differences between the two metals were observed in the effect of the pH (Figure 5c,f). It can be seen that the CP/SWCNTs/Ni−N−C had a different dependence on the pH than the CP/SWCNTs/Cu−N−C. The optimal pH for the degradation of the CP/SWCNTs/Ni−N−C was found to be 3, whereas the optimal pH for the CP/SWCNTs/Cu−N−C was 1. Atomic Ni has been reported to show a direct dechlorination mechanism on CAAs,[18] but herein, the atomic Ni composite electrode was unable to dechlorinate dichloroacetic acid or monochloroacetic acid (Figure S5c,d). We hypothesize that CP/SWCNTs/Ni−N−C does not employ a direct dechlorination mechanism but rather undergoes H*-mediated dechlorination. This hypothesis was confirmed by the pH effect, as dechlorination occurred consistently from pH = 7 to 3, showing a typical dependence on the hydrogen ion concentration. Another hypothesis regarding dechlorination on the Ni−N−C composites involved the adsorption of chlorophenols on the SWCNTs. Due to high acidity, the increase in hydrogen attached to the surface and the released hydrogen gas prevented the adsorption of chlorophenol on SWCNTs. Thus, the degradation efficiency at pH = 1 was not as good as that at pH = 3. Meanwhile, the CP/SWCNTs/Ni−N−C electrode also degraded pure phenol at pH = 3 (Figure

https://doi.org/10.1021/acsomega.4c04289
ACS Omega 2024, 9, 37910−37922

S5a). The degradation of 4-CP on the CP/SWCNTs/Ni−N−C electrode was analyzed through LC and GC-MS. Phenol was found, and the unbalanced total carbon (Figure 5a) showed the presence of other potential degradation compounds; however, neither cyclohexanone or cyclohexanol was found in GC-MS. Our previous reports have identified cyclohexanone and cyclohexanol as degradation products resulting from a direct dechlorination mechanism.[23] The absence of these compounds further confirmed the hypothesis of the occurrence of H*-mediated dechlorination. The EF was identified as the primary mechanism for phenol degradation on the electrodes. These results prove that the CP/SWCNTs/Ni−N−C underwent a combined reaction of adsorption, hydrogen reduction, dechlorination, and EF oxidation degradation.

We have previously reported that the weak pi−pi adsorption between copper and benzene rings on COPs promoted direct electron transfer between a ball-milled metal and the degradation products.[25] This type of adsorption could occur between SWCNTs and aromatic COPs to accelerate the degradation. To verify this hypothesis, CP/SWCNTs/Ni−N−C was used for the degradation of 2,4-DCP and benzene-free COPs (monochloroacetic acid and dichloroacetic acid). As shown in Figure S5b, the initial degradation product of 2,4-DCP was identified as 2-CP, which subsequently underwent further degradation. The results also proved the existence of HRD. CPs were initially eliminated by HRD, as indicated by the 2-CP concentration initially showing an increase and then a decrease. 2-CP is a typical reduction product of HRD; the EF was then involved in the degradation process. However, neither monochloroacetic acid nor dichloroacetic acid was dechlorinated, and even phenol was degraded by the Ni−N−C-modified electrode. This means that pi−pi adsorption was important for HRD in the CP/SWCNTs/Ni−N−C degradation, adsorption, reduction (HRD), and oxidation (EF) process.

To confirm the EF mechanism, the oxygen content of the reaction system was changed to compare the degradation differences. The comparison showed that during the degradation under nitrogen protection without oxygen pumped in, the nitrogen protection reduced the degradation rate from 100 to 20% (reaction time of 2 h) by the CP/SWCNTs/Ni−N−C (Figure 6a), and the degradation rate for the CP/SWCNTs/Cu−N−C system decreased from 76 to 23%. Oxygen is important for the reaction system, so the EF was one of the important means of degrading 4-CP by the cathode. However, there was still a weak degradation efficiency under nitrogen protection. It is speculated that the HRD during the degradation process was also ongoing. Hydroxyl radicals (·OH) are a main component of the EF. To investigate the presence of ·OH, reagents for capturing hydroxyl radicals, including TBA, *p*-benzoquinone, and sodium thiocyanate (NaSCN), were added.

TBA had the effect of eliminating the active hydrogen. With the addition of different concentrations, degradation significantly decreased. Negligible effects were observed with the addition of TBA to the Cu−N−C-modified electrode, and degradation was deduced from 55 to 40%. For the Ni−N−C-modified electrode, the change was more severe, from 90 to 45% (Figure 6b). The degradation was calculated by using Formula 2.

$$\text{degradation rate} = (1 - C_t/C_0) \times 100\% \quad (2)$$

The same results were obtained for *p*-benzoquinone as an ·OH and $\cdot O_2$ capturer. The degradation of 4-CP for the metal−N−C-modified electrodes decreased, and the decrease for Ni−N−C was more significant (Figure 6d). This result shows that ·OH played an important role in 4-CP removal on the CP/SWCNTs/Ni−N−C, and Ni−N−C had a greater ability to form ·OH than Cu−N−C. This was the reason that the main degradation component for CP/SWCNTs/Cu−N−C was phenol, as shown in Figure 5e. Different mechanisms were involved for the Ni−N−C- and Cu−N−C-modified electrodes. It has been reported that atomic Fe has the ability to form ·OH. Herein, we found that atomic Ni also has a strong ability to form ·OH, while simultaneously showing an ability to induce an HRD reaction; the combination of these two abilities is the reason behind the excellent degradation effect found in CP/SWCNTs/Ni−N−C.

Interestingly, when the TBA concentration was further increased to 500 mM, the degradation efficiency of 4-CP remained almost unchanged (Figure 6b). This result showed that even though all ·OH radicals were trapped by TBA, this corresponded only to 45−50% of 4-CP removal. It indicates another process for 4-CP degradation in addition to ·OH oxidation, confirming the occurrence of the HRD reaction.

The intermediates of 4-CP degradation were determined using gas chromatography−mass spectrometry (GC-MS) and HPLC. Phenol appeared at both metal−N−C electrodes, indicating that the HRD reaction occurred at both electrodes. However, phenol was not effectively degraded further at the Cu−N−C-modified electrode at pH = 5. Based on the strong ability for the EF to occur, the Ni−N−C-modified electrode could further degrade phenol for mineralization. The Ni−N−C promoted the formation of H*, and H* was reported to activate H_2O_2 to form ·OH.[26]

To confirm the different mechanisms for the two metal−N−C samples, NaSCN was added to the reactions. SCN^- could poison the metal active centers, as reported previously. SCN^--poisoning experiments were performed, and a decrease in the degradation of 4-CP was observed, indicating that the metal−N−C provided the main active sites (Figure 6c). Based on this inference, the entire degradation process of 4-CP on the CP/SWCNTs/Ni−N−C was speculated to be 4-CP adsorbing on the SWCNTs, then being dechlorinated by H* on the Ni−N−C. The dechlorination products were further oxidized and mineralized by ·OH, and ·OH was produced from H_2O_2, and the Ni−N−C as the point to activate the H_2O_2. H_2O_2 was generated on N-doped graphene or SWCNTs (Figure 8).

The oxygen evolution of the CP/SWCNTs/Ni−N−C was conducted through LSV experiments (Figure S4b). At a current density of +0.01 A, it can be seen that the oxygen evolution potential of the CP/SWCNTs/Ni−N−C was the smallest at +1.0 V. For the CP, CP/SWCNTs, and CP/SWCNTs/Ni−N−C, the potentials were +1.2, + 1.3, and +1.6 V, respectively, and CP/SWCNTs/Ni−N−C was demonstrated with best oxygen reduction activity (ORR). However, this result was inconsistent with the generated H_2O_2.

Meanwhile, the CP/SWCNTs/Ni−N−C had the highest hydrogen evolution current at −1.45 V(a current density of −0.02 A), and the result was consistent with its dechlorination ability, shown is Figure 4a,b.

The reactive oxygen species were measured using EPR with 5,5-dimethyl-1-pyrroline-*x*-oxide (DMPO) as a probe (Figure 6e). Four characteristic peaks with an intensity ratio of 1:2:2:1, which were related to DMPO-·OH, were observed on the four

https://doi.org/10.1021/acsomega.4c04289
ACS Omega 2024, 9, 37910−37922

Table 1. Single-Atom Materials in the Electrochemical Degradation of Organic Chlorinated Pollutants Have Been Reported Recently[a]

single-atom material	degradation mechanism	aim pollutants	K_{obs}/metal mass	citations
Fe/Co bimetal	electric Fenton	COD		13
Co	reduction−oxidation	2,4-dichlorophenoxyacetic acid	546.4 $min^{-1}·g\ metal^{-1}$	32
Fe/Cu bimetallic	reduction−oxidation	4-CP	545.1−137 $min^{-1}·g\ metal^{-1}$	11
Fe	hydrodichlorination	trichloroacetamide		34
Pd	hydrodichlorination	4-CP	9 mmol · g^{-1} ·h^{-1}	35
Pd	hydrodichlorination	chlorophenols		2
Ni	hydrodichlorination	chloroacetic acids		36
Ni complex with SWCNTs	eduction−oxidation	chlorophenols	1956.5 $min^{-1}g^{-1}$	this paper

[a]Dechlorination activity

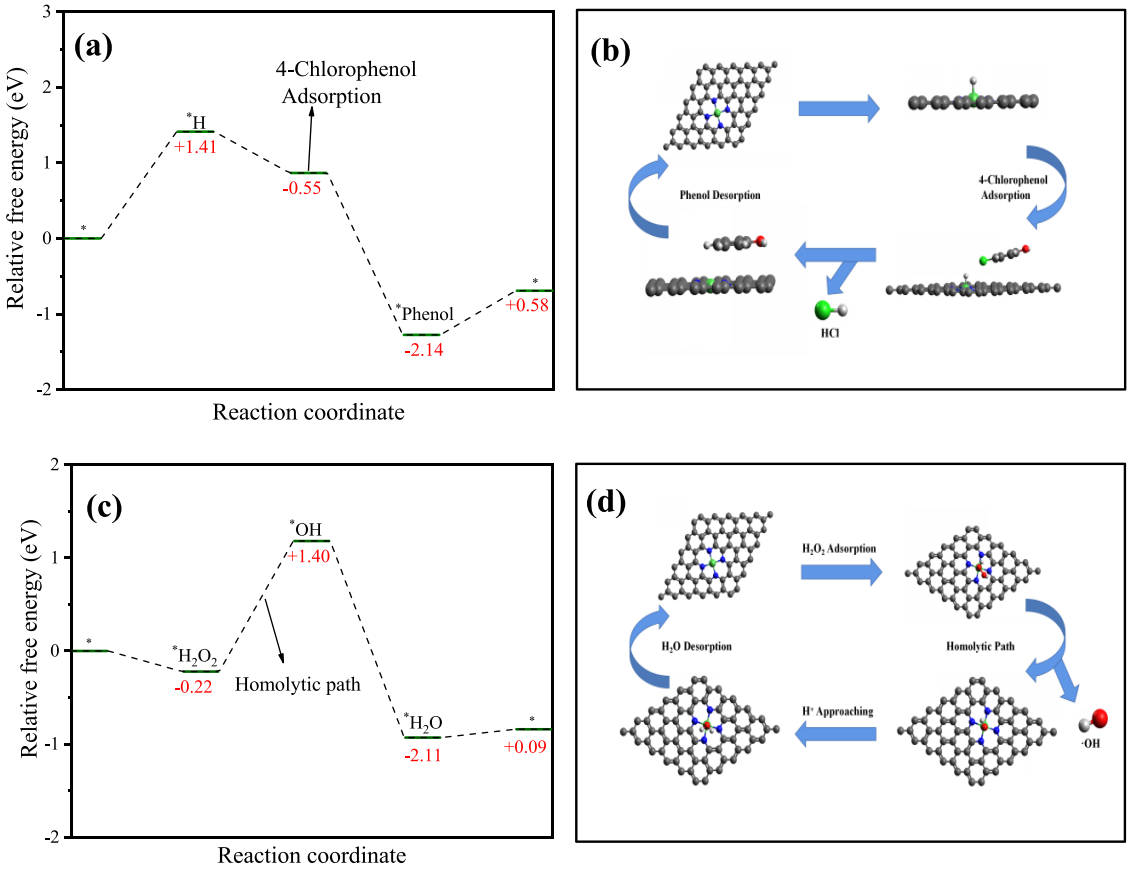

Figure 7. (a, b) Free-energy variation for the conversion of 4-chlorophenol to phenol on the Ni−N_4−C surface and (c, d) free-energy variation for hydroxyl radical generation from hydrogen peroxide on the Ni−N_4−C surface.

electrodes. The CP/SWCNTs/Ni−N−C yielded the highest concentration of ·OH, but the CP/SWCNTs yielded the highest concentration of H_2O_2 (Figure 6f). This abnormal result was attributed to the H* caused by Ni−N−C exhibiting an activation effect on H_2O_2 to decompose it to ·OH, promoting the forward progress of the ORR reaction.[26]

$$H^+ + 1e^- \xrightarrow{\text{Ni-N-C}} H^* \quad (3)$$

$$H^* + H_2O_2 \rightarrow \cdot OH + H_2O \quad (4)$$

This result was consistent with the previous reports, indicating that the SWCNTs could promote the generation of H_2O_2.[2,6] The SWCNTs could not effectively promote the decomposition of H_2O_2, but the Ni−N−C or Cu−N−C could decompose it and promote the generation of •OH. Thus, the order of the peak concentrations of ·OH formed by four electrodes was CP/N−C < CP/SWCNTs < CP/SWCNTs/Cu−N−C < CP/SWCNTs/Ni−N−C. This result was consistent with the dechlorination of 4-CP shown in Figure 4b, and the K_{obs} for 4-CP degradation on the CP/SWCNTs/Ni−N−C was higher than that on the CP/SWCNTs. Herein, SWCNTs serve dual roles in electrode composites: the absorption of CPs and the promotion of H_2O_2 generation.

The degradation experiment for 4-CP using CP/SWCNTs/Ni−N−C was conducted for 2 h, and the degradation rate of 4-CP exceeded 90%. The 4-CP was completely dechlorinated and degraded; however, the degradation of total organic carbon (TOC) was only 30%, which was consistent with the results for ·OH oxidation by the EF, indicating a low-mineralization ability. Meanwhile, the degradation of TOC on CP/SWCNTs/Cu−N−C was only 8%, indicating the substantial difference between it and CP/SWCNTs/Ni−N−

https://doi.org/10.1021/acsomega.4c04289
ACS Omega 2024, 9, 37910−37922

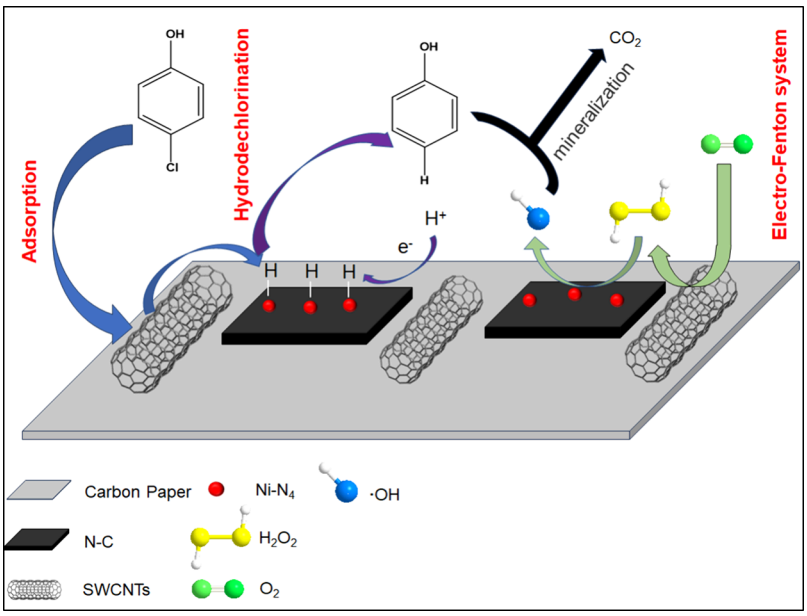

Figure 8. Mechanism of elimination for 4-CP on CP/SWCNTs/Ni−N−C.

C and demonstrating a novel pathway for the Ni−N−C electrode. The SOS/umu test (see the Supporting Information) with 30 ppm 4-CP and its degraded solution showed that the I_R values of the degraded solution were both lower than the positive reference value. The I_R values of the degraded solution decreased from the initial 1.43 to 1.11 and 1.02 after 2 and 5 h of degradation, respectively. The toxicity values decreased during the reaction. The degradation products showed no risk of toxicity. Therefore, the CP/SWCNTs/Ni−N−C was used for HRD complexing with the EF to degrade 4-CP. As shown in Table 1, the material has been found to have a high K_{obs}/metal mass ratio in recent studies.

The stability and reusability of the CP/SWCNTs/Ni−N−C were evaluated by performing a 20 h electrolysis experiment of 10 successive bath treatments at −0.8 V with an initial pH of 3. It showed a steady electrolysis current with a negligible decrease, suggesting the excellent stability of the Ni−N−C complex with SWCNTs for long-term operation; the degradation remained almost constant in each cycle. Undetectable levels of Ni metallic ions were measured for each cycle using ICP-AES, and after its usage, the TEM and SEM-EDS results showed that the morphology and Ni contents remained unchanged compared with those before its usage. The phenomena demonstrated that Ni−N−C complexed with SWCNTs acted as a stable catalyst in the EF for COP removal. The material showed good stability and reusability in the treatment of COP wastewater.

3.3. Degradation Reaction Mechanism. The EF mechanism of the electrode was analyzed in detail. The degradation of COPs over the CP/SWCNTs/Ni−N−C occurred via HRD and the EF. Under weakly acidic conditions (pH = 3), the benzene ring structure of aromatic COPs conjugated with carbon-based materials, causing the activation of hydrogen on the Ni−N−C for the dechlorination of COPs. Simultaneously, the ORR reaction occurred on COPs or SWCNTs, forming H_2O_2. The Ni−N−C sites promoted the formation of ·OH (EF) and continually converted the dechlorination product phenol to small molecules for complete degradation.

For investigating the roles of single-atom Ni and SWCNTs of degrading 4-CP, theoretical calculations were conducted using the first-principles program CP2K 2023. Based on the EXAFS result, the single-atom Ni was coordinated with four N atoms in the Ni−N−C model, and a single-atom Ni was anchored with four N atoms, denoted as Ni−N_4. The absorption energies of H* and 4-CP on carbon-based and atomic metal surfaces were calculated (Figure 7a). The negative absorption energy indicated that the reactant adsorption was favorable in the model. The O_2 adsorption energies on Ni−N_4 and N−C were −0.22 and −0.53 V, respectively. This indicates that N−C was beneficial for O_2 adsorption, but less activation occurred by Ni−N_4 than by N−C. This means that Ni−N_4 was the key activation location for ·OH formation.

The free-energy changes during the conversion of 4-CP to phenol on the Ni−N_4−C surface are depicted in Figure 7a. The free-energy changes for the generation of hydroxyl radicals from hydrogen peroxide on the Ni−N_4−C surface are shown in Figure 7b. The free-energy changes of the generation of hydroxyl radicals from hydrogen peroxide on the N_4−C surface are shown in Figure 7c,d. O_2 adsorption on the N−C was favorable, resulting in the formation of H_2O_2, which was activated to ·OH on the Ni−N_4. Furthermore, 4-CP adsorption on the SWCNTs was favorable (Figure S6), and H* was formed and adsorbed on the Ni−N_4. The DFT calculations were consistent with the experiment results.

The DFT calculations and experimental results revealed that the synergistic effect between dechlorination adsorption on Ni−N−C and SWCNT and oxidation of EF and −OH enhances the removal of 4-CP. As discussed earlier, Ni−N_4 in porous carbon significantly improved the ORR activity, where the single-atom Ni not only accelerated 4-CP hydrogen reduction dechlorination but also facilitated ·OH radical production from H_2O_2. H_2O_2 was produced from the reduction of the O_2 on the N−C or SWCNTs. Therefore, the enhanced EF activity of 4-CP degradation on Ni−N−C and SWCNT may be due to the atomic distribution of nickel

https://doi.org/10.1021/acsomega.4c04289
ACS Omega 2024, 9, 37910−37922

as well as the π-bonding on SWCNT or nitrogen-doped graphene. Figure 8 shows the degradation mechanism.

Meanwhile, H* adsorbed onto the surface of Ni−N_4 and 4-CP adsorbed onto the SWCNTs, and then, dechlorination occurred with H*. O_2 was adsorbed on the N−C or SWCNTs and was formed to H_2O_2 through a two-electron ORR pathway. The formed H_2O_2 preferentially adsorbed on the single-atom Ni and decomposed to the ·OH radicals. As a result, 4-CP at the electrode can be dechlorinated and removed by dechlorination reduction and EF with kinetic constants as high as 2.7 h^{-1}, which is much higher than those of the Ni−N−C- and SWCNT-modified electrodes. The metal mass kinetics constant was 1956.5 $min^{-1}g^{-1}$, which is even higher than that reported for FeCuSA-NPC. These results showed that metal Ni has EF activity[37] comparable to that of metal Fe.[11] While atomic Pd has been reported to generate H*, few inexpensive metals have been reported to possess this ability. Meanwhile, Ni nanoparticles have been reported to generate H* for dechlorination.[38] In this study, atomic Ni showed not only HRD activity but also EF activity. This new mechanism contributed to it having the highest metal mass kinetics constant.

4. CONCLUSIONS

Atomic Ni anchored on N-doped carbon was complexed with SWCNTs to produce electrochemical cathodes as trifunctional electrodes to remove COP by adsorption, HRD, and EF. The performance and mechanism of degradation of 4-CP were studied in detail. The H* on Ni−N−C, COP adsorption on the SWCNTs, and ·OH radicals were responsible for the efficient degradation. DFT calculations indicated that the N−C showed the $2e^-$ ORR to increase the performance and the Ni−N_4 decomposes H_2O_2 to ·OH via a $1e^-$ process. The CP/SWCNTs/Ni−N−C electrocatalytic system completely dechlorinated 4-CP in 2 h; the TOC significantly decreased, and biological toxicity decreased. Benefiting from the synergistic effects of the Ni−N−C and SWCNTs, the kinetics constant of the electrode for 4-CP removal reached 2.7 h^{-1} and 1956.5 $min^{-1}g^{-1}$. We designed a single-atom metal electrode with three functional effects for the degradation of COPs for the first time. This experiment provides a new perspective for the fabrication of highly active multifunctional electrocatalysts for the degradation of COPs in water.

■ ASSOCIATED CONTENT

Supporting Information

The Supporting Information is available free of charge at https://pubs.acs.org/doi/10.1021/acsomega.4c04289.

Supplementary experimental section, supplementary figures and tables, and supplementary references (PDF)

■ AUTHOR INFORMATION

Corresponding Authors

Hong Zhu − *Key Laboratory of Urban Agriculture In North China, Ministry of Agriculture and Rural Affairs, P.R.China, Beijing University of Agriculture, Beijing 102206, P.R. China;* orcid.org/0000-0001-8178-1926; Email: zhuhong80@pku.edu.cn

Xiaoxiong Huang − *State Key Laboratory of Molecular Engineering of Polymers, Department of Macromolecular Science, Fudan University, Shanghai 200438, P. R. China;* Email: huangxx20210530@163.com

Authors

Xinlong Pei − *Key Laboratory of Urban Agriculture In North China, Ministry of Agriculture and Rural Affairs, P.R.China, Beijing University of Agriculture, Beijing 102206, P.R. China*

Baitao Chen − *Key Laboratory of Urban Agriculture In North China, Ministry of Agriculture and Rural Affairs, P.R.China, Beijing University of Agriculture, Beijing 102206, P.R. China*

Zehui Wang − *Key Laboratory of Urban Agriculture In North China, Ministry of Agriculture and Rural Affairs, P.R.China, Beijing University of Agriculture, Beijing 102206, P.R. China*

Chenhong Ma − *Key Laboratory of Urban Agriculture In North China, Ministry of Agriculture and Rural Affairs, P.R.China, Beijing University of Agriculture, Beijing 102206, P.R. China*

Long Li − *Key Laboratory of Urban Agriculture In North China, Ministry of Agriculture and Rural Affairs, P.R.China, Beijing University of Agriculture, Beijing 102206, P.R. China*

Yonghong Li − *Key Laboratory of Environmental Factors and Chronic Disease Control, School of Public Health, Ningxia Medical University, Yinchuan 750004, P.R. China*

Xiaolong Yao − *Department of Environment Science and Engineering, Beijing Technology and Business University, Beijing 100048, China;* orcid.org/0000-0003-3459-7813

Complete contact information is available at: https://pubs.acs.org/10.1021/acsomega.4c04289

Author Contributions

$^{\perp}$X.P. and B.C. contributed equally to this work

Notes

The authors declare no competing financial interest.

■ ACKNOWLEDGMENTS

This work was supported by the National Nature Science Foundation of China (project nos. 52100116 and 21207077), Urban Agriculture and Forestry Emerging Interdisciplinary Platform Project, Science and Technology innovation support program of Beijing University of Agriculture, the Fund of the Key Laboratory of Urban Agriculture in North China (project no. KFKT-2024008), Ministry of Agriculture and Rural Affairs, P.R. China, and Beijing University of Agriculture, Beijing 102206, P.R. China.

■ REFERENCES

(1) Lei, C.; Liang, F.; Li, J.; Chen, W.; Huang, B. Electrochemical reductive dechlorination of chlorinated volatile organic compounds (Cl-VOCs): Effects of molecular structure on the dehalogenation reactivity and mechanisms. *Chemical Engineering Journal* **2019**, *358*, 1054−1064.

(2) Chu, C.; Huang, D.; Gupta, S.; Weon, S.; Niu, J.; Stavitski, E.; Muhich, C.; Kim, J. H. Neighboring Pd single atoms surpass isolated single atoms for selective hydrodehalogenation catalysis. *Nat. Commun.* **2021**, *12* (1), 5179.

(3) Feng, L.; Ge, X.; Li, Y.; Wang, D.; Tang, H. Dechlorination of 2, 4-dichlorophenol by nickel nanoparticles under the acidic conditions. *Chin. Sci. Bull.* **2011**, *56*, 2258−2266.

(4) Lv, X.; Prastistho, W.; Yang, Q.; Tokoro, C. Application of nano-scale zero-valent iron adsorbed on magnetite nanoparticles for removal of carbon tetrachloride: Products and degradation pathway. *Appl. Organomet. Chem.* **2020**, *34* (5), No. e5592.

(5) Chaplin, B. P.; Schrader, G.; Farrell, J. Electrochemical oxidation of N-nitrosodimethylamine with boron-doped diamond film electrodes. *Environ. Sci. Technol.* **2009**, *43* (21), 8302−8307.
(6) Durante, C.; Perazzolo, V.; Isse, A. A.; Favaro, M.; Granozzi, G.; Gennaro, A. Electrochemical activation of carbon−halogen bonds: electrocatalysis at palladium−copper nanoparticles. *ChemElectroChem.* **2014**, *1* (8), 1370−1381.
(7) Mao, R.; Zhao, X.; Lan, H. C.; Liu, H. J.; Qu, J. H. Efficient electrochemical reduction of bromate by a Pd/rGO/CFP electrode with low applied potentials. *Appl. Catal., B* **2014**, *160*, 179−187.
(8) Carter, K. E.; Farrell, J. Electrochemical Oxidation of Trichloroethylene Using Boron-Doped Diamond Film Electrodes. *Environ. Sci. Technol.* **2009**, *43* (21), 8350−8354.
(9) Gan, G.; Fan, S.; Li, X.; Wang, J.; Bai, C.; Guo, X.; Tade, M.; Liu, S. Nature of intrinsic defects in carbon materials for electrochemical dechlorination of 1, 2-dichloroethane to ethylene. *ACS Catal.* **2021**, *11* (22), 14284−14292.
(10) Tang, H.; Bian, Z.; Peng, Y.; Li, S.; Wang, H. Stepwise dechlorination of chlorinated alkenes on an Fe-Ni/rGO/Ni foam cathode: Product control by one-electron-transfer reactions. *Journal of Hazardous Materials* **2022**, *433*, No. 128744.
(11) Zhao, K.; Quan, X.; Su, Y.; Qin, X.; Chen, S.; Yu, H. Enhanced Chlorinated Pollutant Degradation by the Synergistic Effect between Dechlorination and Hydroxyl Radical Oxidation on a Bimetallic Single-Atom Catalyst. *Environ. Sci. Technol.* **2021**, *55* (20), 14194−14203.
(12) Lee, H.-J.; Zhang, N.; Ganzoury, M. A.; Wu, Y.; de Lannoy, C.-F. Simultaneous dechlorination and advanced oxidation using electrically conductive carbon nanotube membranes. *ACS Appl. Mater. Interfaces* **2021**, *13* (29), 34084−34092.
(13) Qin, X.; Cao, P.; Quan, X.; Zhao, K.; Chen, S.; Yu, H.; Su, Y. Highly efficient hydroxyl radicals production boosted by the atomically dispersed Fe and Co sites for heterogeneous electro-Fenton oxidation. *Environ. Sci. Technol.* **2023**, *57* (7), 2907−2917.
(14) Wang, W.; Cao, Y.; Hu, X.; Zhou, S.; Zhu, D.; Qi, D.; Deng, S. Granular reduced graphene oxide/Fe3O4 hydrogel for efficient adsorption and catalytic oxidation of p-perfluorous nonenoxybenzene sulfonate. *Journal of hazardous materials* **2020**, *386*, No. 121662.
(15) Yang, K.; Kong, Y.-J.; Huang, L.-Z.; Hu, X.-M. Catalytic elimination of chlorinated organic pollutants by emerging single-atom catalysts. *Chemical Engineering Journal* **2022**, *450*, No. 138467.
(16) Williams, C. K.; McCarver, G. A.; Lashgari, A.; Vogiatzis, K. D.; Jiang, J. J. Electrocatalytic dechlorination of dichloromethane in water using a heterogenized molecular copper complex. *Inorg. Chem.* **2021**, *60* (7), 4915−4923.
(17) Zhou, J.; Lou, Z.; Wang, Z.; Zhou, C.; Li, C.; Ali Baig, S.; Xu, X. Electrocatalytic dechlorination of 2, 4-DCBA using CTAB functionalized Pd/GAC movable granular catalyst: Role of adsorption in catalysis. *Chemical Engineering Journal* **2021**, *414*, No. 128758.
(18) Xu, Y.; Yao, Z.; Mao, Z.; Shi, M.; Zhang, X.; Cheng, F.; Yang, H. B.; Tao, H. B.; Liu, B. Single-Ni-atom catalyzes aqueous phase electrochemical reductive dechlorination reaction. *Applied Catalysis B: Environmental* **2020**, *277*, No. 119057.
(19) Li, N.; Song, X.; Wang, L.; Geng, X.; Wang, H.; Tang, H.; Bian, Z. Single-atom cobalt catalysts for electrocatalytic hydrodechlorination and oxygen reduction reaction for the degradation of chlorinated organic compounds. *ACS Appl. Mater. Interfaces* **2020**, *12* (21), 24019−24029.
(20) Gan, G.; Li, X.; Wang, L.; Fan, S.; Mu, J.; Wang, P.; Chen, G. Active sites in single-atom Fe−N x−C nanosheets for selective electrochemical dechlorination of 1, 2-dichloroethane to ethylene. *ACS Nano* **2020**, *14* (8), 9929.
(21) Wen, F.; Zhang, F.; Liu, Z. Investigation on Microwave Absorption Properties for Multiwalled Carbon Nanotubes/Fe/Co/Ni Nanopowders as Lightweight Absorbers. *J. Phys. Chem. C* **2011**, *115* (29), 14025−14030.
(22) Gan, T.; Wang, D. Atomically dispersed materials: Ideal catalysts in atomic era. *Nano Research* **2024**, *17* (1), 18−38.
(23) Yang, X.; Cheng, J.; Li, H.; Xu, Y.; Tu, W.; Zhou, J. Self-supported N-doped hierarchical Co3O4 electrocatalyst with abundant oxygen vacancies for acidic water oxidation. *Chemical Engineering Journal* **2023**, *465*, No. 142745.
(24) Wang, X. Y.; Pan, Y. Z.; Yang, J.; Li, W. H.; Gan, T.; Pan, Y. M.; Tang, H. T.; Wang, D. Single-Atom Iron Catalyst as an Advanced Redox Mediator for Anodic Oxidation of Organic Electrosynthesis. *Angew. Chem.* **2024**, No. e202404295.
(25) Duan, J.; Zhu, H.; Xu, F.; Zhao, J. A new approach to 4-chlorophenol dechlorination on monometallic copper compared to its Cu/Fe bimetallic system. *Chemical Engineering Journal* **2016**, *304*, 282−288.
(26) Wang, K.; Cao, P.; Qin, X.; Chen, S.; Yu, H.; Quan, X. Electro-Fenton process with scalable modified carbonaceous electrode material processed by direct calcination for refractory organic pollutant degradation. *Chemical Engineering Journal* **2023**, *470*, No. 144104.
(27) Cheng, H.; Wen, Y.; Huang, C.; Wang, P.; Sun, C.; Feng, C.; Xu, J.; Du, L.; Yan, T.; Cheng, M. Application of Mo2C for enhancement of co-catalytic performance of Fe3+/PS based fenton-like reaction in degrading tetracycline hydrochloride. *Chemical Engineering Journal* **2023**, *474*, No. 145508.
(28) Zeng, H.; Zhang, G.; Ji, Q.; Liu, H.; Hua, X.; Xia, H.; Sillanpää, M.; Qu, J. pH-Independent Production of Hydroxyl Radical from Atomic H*-Mediated Electrocatalytic H2O2 Reduction: A Green Fenton Process without Byproducts. *Environ. Sci. Technol.* **2020**, *54* (22), 14725−14731.
(29) Guan, A.; Chen, Z.; Quan, Y.; Peng, C.; Wang, Z.; Sham, T.-K.; Yang, C.; Ji, Y.; Qian, L.; Xu, X.; Zheng, G. Boosting CO2 Electroreduction to CH4 via Tuning Neighboring Single-Copper Sites. *ACS Energy Letters* **2020**, *5* (4), 1044−1053.
(30) Zhou, M.; Jiang, Y.; Wang, G.; Wu, W.; Chen, W.; Yu, P.; Lin, Y.; Mao, J.; Mao, L. Single-atom Ni-N4 provides a robust cellular NO sensor. *Nat. Commun.* **2020**, *11* (1), 3188.
(31) Hou, Y.; Liang, Y.-L.; Shi, P.-C.; Huang, Y.-B.; Cao, R. Atomically dispersed Ni species on N-doped carbon nanotubes for electroreduction of CO2 with nearly 100% CO selectivity. *Applied Catalysis B: Environmental* **2020**, *271*, No. 118929.
(32) Liu, L.; Chen, Y.; Li, S.; Yu, W.; Zhang, X.; Wang, H.; Ren, J.; Bian, Z. Enhanced electrocatalytic cathodic degradation of 2,4-dichlorophenoxyacetic acid based on a synergistic effect obtained from Co single atoms and Cu nanoclusters. *Applied Catalysis B: Environmental* **2023**, *332*, No. 122748.
(33) Li, J.; Zhang, C.; Li, Y.; Pan, Y.; Liu, Y. Rational Design and Structural Regulation of Robust Catalysts for Electrocatalytic Hydrodechlorination: From Nanostructures to Single Atoms. *ACS Catal.* **2023**, *13* (14), 9633−9655.
(34) Lou, Y.-Y.; Yin, S.-H.; Yang, J.; Ji, L.-F.; Fang, J.-Y.; Zhang, S.-Q.; Feng, M.-B.; Yu, X.; Jiang, Y.-X.; Sun, S.-G. MOF-derived single site catalysts with Electron-Rich Fe-N4 sites for efficient elimination of trichloroacetamide DBP. *Chemical Engineering Journal* **2022**, *446*, No. 137060.
(35) Mao, Z.; Liu, L.; Yang, H. B.; Zhang, Y.; Yao, Z.; Wu, H.; Huang, Y.; Xu, Y.; Liu, B. Atomically dispersed Pd electrocatalyst for efficient aqueous phase dechlorination reaction. *Electrochim. Acta* **2021**, *391*, No. 138886.
(36) Xu, Y.; Yao, Z.; Mao, Z.; Shi, M.; Zhang, X.; Cheng, F.; Yang, H. B.; Bing Tao, H.; Liu, B. Single-Ni-Atom Catalyzes Aqueous Phase Electrochemical Reductive Dechlorination Reaction. *Appl. Catal., B* **2020**, No. 119057.
(37) Huang, D.; Kim, D. J.; Rigby, K.; Zhou, X.; Wu, X.; Meese, A.; Niu, J.; Stavitski, E.; Kim, J. H. Elucidating the Role of Single-Atom Pd for Electrocatalytic Hydrodechlorination. *Environ. Sci. Technol.* **2021**, *55* (19), 13306−13316.
(38) Wang, Q.; Du, J.; Ma, Y.-Y.; Yin, X.-Y.; Tian, Z.-Y.; Han, Z.-G. Noble-metal-free 3D hierarchical Ni-WC heterostructure with enhanced interfacial charge transfer for efficient electrocatalytic hydrodechlorination. *Chemical Engineering Journal* **2023**, *451*, No. 139107.

https://doi.org/10.1021/acsomega.4c04289
ACS Omega 2024, 9, 37910−37922